



Agricultural Burning and Air Quality over Northern India: A Synergistic Analysis using NASA's A-train Satellite Data and Ground Measurements

Hiren Jethva^{1,2*}, Duli Chand³, Omar Torres², Pawan Gupta^{1,2}, Alexei Lyapustin²,
Falguni Patadia^{4,2}

¹ Universities Space Research Association, Columbia, MD 21044, USA

² NASA Goddard Space Flight Center, Greenbelt, MD 20771, USA

³ Pacific Northwest National Laboratory, Richland, WA 99352, USA

⁴ Morgan State University, Baltimore, MD 21251, USA

ABSTRACT

In the recent years, New Delhi, the capital city of India, has ranked among the most polluted cities in the world regarding its air quality related to the submicron Particulate Matter ($PM_{2.5}$). Using NASA's A-train satellite data (MODIS, OMI, and CALIOP), ground-level $PM_{2.5}$ measured in New Delhi (2013–2016), and back-trajectory calculations, we show that the $PM_{2.5}$ over New Delhi is strongly affected by the agricultural fires in the northwestern Indian states of Punjab and Haryana during the post-monsoon season (October and November). The mass concentration of $PM_{2.5}$ escalates from ~50 $\mu\text{g m}^{-3}$ measured prior to the onset of residue burning in early October to as high as 300 $\mu\text{g m}^{-3}$ (24-hour averaged, 7-day running mean) during the peak burning period in early November. A linear regression analysis reveals that the variations in $PM_{2.5}$ over New Delhi can be attributed to the concurrent changes in the satellite retrievals of fire counts and aerosols over the crop burning area. The back-trajectory analysis shows that most clusters (> 80%) of the northwesterly flow near the ground intercepted the crop burning region before arriving at the receptor location in New Delhi; this further corroborates the transport patterns inferred from the satellite data. A 15-year long satellite record (2002–2016) reveals an increasing trend in agricultural fires (~617 per year) and aerosol loading (0.031 and 0.04 per year in aerosol optical depth and UV aerosol index) in November. Increasing levels of crop residue burning and resulting particulate matter pollution at an alarming rate over northern India is a pressing concern demanding corrective measures to substantially reduce or completely diminish the crop burning through an effective residue management system.

Keywords: Crop residue fires; Smoke particles; NASA's A-train satellites; $PM_{2.5}$; Northern India.

INTRODUCTION

Biomass burning, including wildfires and open field agricultural burning, poses a serious threat to the climate and air quality. Particulate matter, greenhouse gases, and other air pollutants produced by these activities have a high potential to alter the radiation balance of the Earth, trigger changes in atmospheric chemistry, and can affect the air quality and human health (Stocker *et al.*, 2013). According to the latest World Health Organization (WHO)-Global Urban Ambient Air Pollution Database 2016 (http://www.who.int/phe/health_topics/outdoorair/databases/cities/en/), over 80% of people living in urban areas that monitor air

pollution are exposed to air pollution levels that exceed the WHO limit of 10 $\mu\text{g m}^{-3}$ in $PM_{2.5}$ (annual average). Globally, air pollution (households and outdoor) is the 4th most significant risk factor for deaths, contributing to ~5.5 million premature deaths in 2013; and about 27% of these (~1.51 million) occurred in India alone (Forouzanfar *et al.*, 2015). The 2014 WHO report (<http://www.who.int/phe/en/>) states that 7 million deaths—one in eight of total global deaths, were linked to air pollution in 2012. While there are various measures of the air quality, the particulate matter—fine solid and liquid particles suspended in the air, having an aerodynamic diameter less than 2.5 μm and 10 μm or $PM_{2.5}$ and PM_{10} , have been a widely accepted measure of overall air quality (WHO, 2000). Especially, $PM_{2.5}$ owing to its finer size is more harmful to human health as it can be easily inhaled through the respiratory system, causing serious health problems, including heart, lung diseases, and premature deaths. A number of studies connecting human health and mortality to pollution levels, particularly in

* Corresponding author.

Tel.: 1-301-614-5225

E-mail address: hiren.t.jethva@nasa.gov

global megacities, have come aplenty (Simpson *et al.*, 2000; TERI, 2001; Leeuwen and Rolaf, 2002; Health Effects Institute, 2004, 2008; Pope III *et al.*, 2009; WHO, 2014; van Donkelaar *et al.*, 2015, and many others).

In the recent years, New Delhi, the capital city of India, in the Indo-Gangetic Plain (IGP), has consistently ranked among the most polluted cities in the world regarding the levels of particulate matter (WHO, 2014, 2016). Rapid urbanization and industrialization in this area have led to elevated concentrations of many pollutants over the region. Satellite-based estimates of $\text{PM}_{2.5}$ derived using Multiangle Imaging Spectroradiometer (MISR) retrieved aerosol optical depth over the Indian subcontinent show that 51% of the subcontinent's 1.4 billion people are exposed to the pollution levels that exceed the WHO's highest annual air quality threshold of $35 \mu\text{g m}^{-3}$ with New Delhi topping the chart with annual mean $\text{PM}_{2.5}$ concentration of $148 \mu\text{g m}^{-3}$ (Dey *et al.*, 2012). Besides the local pollution sources in the National Capital Region (NCR), several studies have shown that air quality over NCR is strongly influenced by the transport of air pollutants from the neighboring regions (Venkataraman *et al.*, 2006; Mishra and Shibata, 2012; Kaskaoutis *et al.*, 2014).

The Indian state of Punjab in the northwestern part of the populous IGP in India is often called the “bread basket” owing to producing two-thirds of the country’s food grains with wheat and rice being the principal crops. The region undergoes two major growing seasons annually, one from May to September followed by rice harvesting during October and November, and another from November to April followed by wheat harvesting in April and May. Prior to mid-1980’s, the farming practice was mostly manual, and the crop residue was allowed to be root-bound for several weeks for allowing mixing with soil and better enrichment of the land for the next crop. Since then, the manual farming practice was replaced by the mechanized harvesting owing to reduced labor and economic benefits (Singh and Kaskaoutis, 2014). However, mechanized harvesting leaves a portion of stalks still root-bound, typically rising about several inches off the ground. Farmers usually burn the crop residue for clearing and preparing the land for the next crop. The burning of agricultural leftover in open fields for crop rotation is a common practice in the northwestern region of IGP (Badrinath *et al.*, 2006). The data retrieved from the National Biomass Resource Assessment (NBRA) Programme (<http://mnre.gov.in/mnre-2010/related-links/resource-assessment/biomass-resource-atlas/>) indicates that about 21 Tg and 10 Tg, i.e., 46% and 37% of the total rice straw produced in the field, is surplus and subject to open field burning in the states of Punjab and Haryana, respectively. According to the national and statewide inventory database for India, the states of Punjab and Haryana rank higher regarding the maximum crop residues burnt and resulting emissions of chemically and radiatively active greenhouse gases and particulate matter (Jain *et al.*, 2014). Several studies have shown using in situ, ground-based and satellite retrievals that the paddy burning during post-monsoon in this region results in elevated concentrations of particulate matter (up to $400 \mu\text{g m}^{-3}$, predominantly composed of organic

carbon) (Rajput *et al.*, 2013) and harmful gases such as NO_2 , SO_2 , and CH_4 (Mittal *et al.*, 2009). Besides its adverse effects on climate and human health, crop residue burning also adversely affects the soil fertility through loss of essential nutrients (Carbon, Nitrogen, and Sulphur), fungi, bacteria, and pests which otherwise are beneficial for the crops.

Fig. 1 shows two case studies of agricultural fires and associated smoke loading over the IGP region for two consecutive days, November 11th and 12th of 2014. The true-color images captured by the Moderate Resolution Imaging Spectroradiometer (MODIS) onboard the Aqua platform are super-imposed with fire spots (red dots) detected by the same sensor following the thermal anomaly detection algorithm (Giglio *et al.*, 2003, 2016). The daily-averaged $\text{PM}_{2.5}$ recorded by the ground instrument downwind of the fires and at the U.S. Embassy site in New Delhi on November 11th was $222 \mu\text{g m}^{-3}$, which then substantially increased to $317 \mu\text{g m}^{-3}$ on the following day. The back-trajectory plot obtained from NOAA’s Hybrid Single Particle Lagrangian Integrated Trajectory model (HYSPLIT) online tool (READY), shown as an inset on the right of Fig. 1, tells that the wind fields near the surface and at 500 m above the ground were northwesterly and intercepted the crop residue burning region before arriving at the receptor location in New Delhi the next day. A visual analysis of the true-color images supported by the back-trajectories unambiguously shows the transport of smoke particles from Punjab is not just limited to New Delhi and surrounding region but occurs over a much larger area of IGP.

Many more case studies similar to the one shown in Fig. 1 motivated to investigate further the impacts of crop residue burning over the northwestern Indian states of Punjab and Haryana on the ground-level concentration of $\text{PM}_{2.5}$ measured at the downwind location of the U.S. Embassy in New Delhi. Satellite measurements of fires and pollution from NASA’s A-train sensors, surface-level $\text{PM}_{2.5}$ mass concentration measured at New Delhi, and back-trajectory data obtained from the NOAA HYSPLIT model provided essential datasets to perform a synergistic analysis. Several studies have highlighted the impacts of agricultural fires in northwestern India on the atmospheric composition and $\text{PM}_{2.5}$ in the region (Badrinath *et al.*, 2006; Venkataraman *et al.*, 2006; Rajput *et al.*, 2013; Jain *et al.*, 2014; Kaskaoutis *et al.*, 2014). However, quantitative and correlative analysis of the ground-satellite measurements that can establish a relationship between the fires and associated smoke particles and $\text{PM}_{2.5}$ has been lacking. For instance, it is desirable to quantify the rate of increase in $\text{PM}_{2.5}$ at a receptor location due to the rise in agricultural fires and aerosol loading over the burning region. Such relationships can form a quantitative basis for the attribution and even the prediction of $\text{PM}_{2.5}$. Furthermore, A-train satellite measurements provide a unique opportunity to investigate the long-term changes in fires and resulting aerosol loading.

The rest of the paper is arranged as follows. A brief description of different datasets employed in the present study is given in section 2; analysis of the time evolution of fires and satellite retrievals, ground versus satellite measurement correlation, vertical distribution of aerosols,

Aqua/MODIS True-color RGB & Thermal Anomalies/Fires

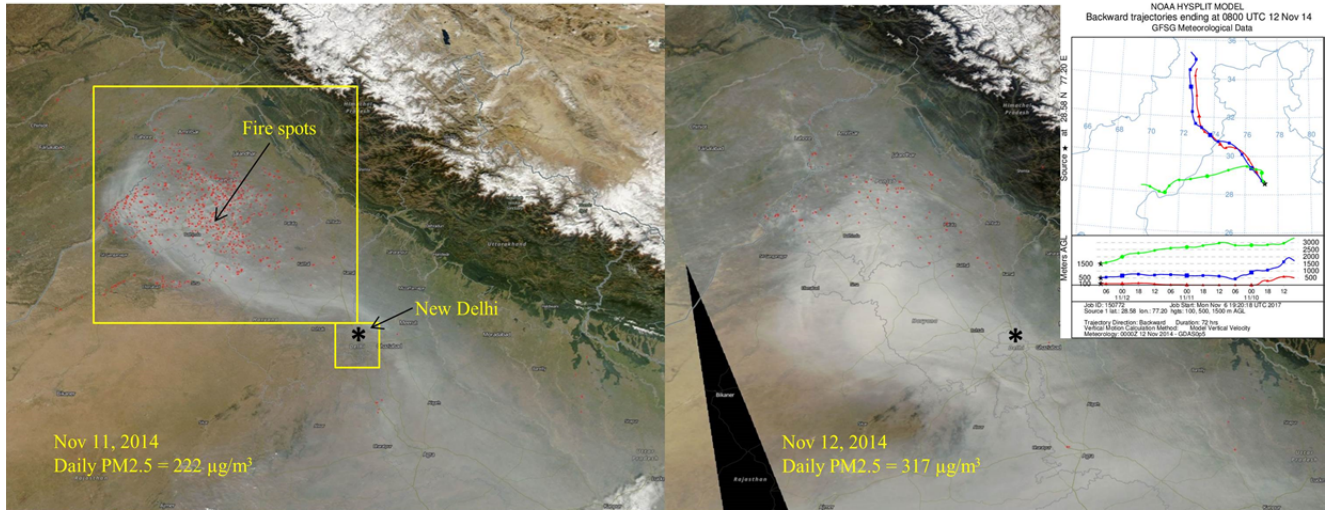


Fig. 1. True-color RGB images super-imposed with thermal anomalies/fires spots detected by Aqua/MODIS over northern India for 11th (left) and 12th (right) November of 2014. The boxes shown on the left are the regions considered in the present analysis. The location of New Delhi is depicted with an asterisk. A three-day back-trajectory ending in New Delhi on Nov 12, 2014, is shown as an inset on the top-right.

back-trajectory data, and long-term record of fires and smoke aerosols are presented in section 3; a discussion on several aspects of the analysis and concluding remarks are given in section 4.

A BRIEF DESCRIPTION OF THE DATASETS

Here, we employ multiple datasets consisting of ground measurements, satellite retrievals, and back-trajectory data to investigate the link between crop residue burning and air quality over northern India. Each dataset offers its unique characteristics regarding their measurements and retrieval approaches at different spatiotemporal scales. The PM_{2.5} data measured at the U.S. Embassy site in New Delhi are measured hourly. On the other hand, Aqua/MODIS and Aura/OMI of the A-train satellite constellation capture snapshots of the region once a day. The repeat cycle of CALIOP lidar onboard CALIPSO satellite is once in 16 days over a particular point on the Earth. Moreover, the native ground pixel size and product resolution differ among sensors. While Table 1 lists datasets and their characteristics employed in the present analysis, a brief description of each dataset is provided below.

Ground-level PM_{2.5} Measurements

Under the Air Quality Monitoring (AQM) program, the U.S. Embassy & Consulates operate PM_{2.5} measuring instrument (i.e., MetOne BAM 1020) in the five metro cities of India (New Delhi, Mumbai, Chennai, Kolkata, and Hyderabad). The measurements of fine particulate matter follow the U.S. Environmental Protection Agency (EPA) federal reference equivalent standard. The U.S. EPA does continuous measurements of PM_{2.5} across the U.S.A. to monitor the concentration of fine particulate matter. PM_{2.5} monitoring program at the Embassy site at foreign locations is

operated by the U.S. Department of State in collaboration with the U.S. EPA. The PM_{2.5} data collected by the U.S. Mission in India, including New Delhi since 2013 are also converted into an air quality index (AQI) using the EPA NowCast Algorithm that can help health-related decision making. The AQM stations installed at the five U.S. Consulates in India consist of BAM-1020 housed in the environmentally controlled weatherproof unit. The unit monitors the concentration of PM_{2.5} by the Beta attenuation method of the ambient air sample on an hourly basis. For the present study, we obtained the hourly PM_{2.5} data acquired during 2013 to 2016 at the U.S. Embassy site in New Delhi from a publicly and freely accessible URL <https://in.usembassy.gov/embassy-consulates/new-delhi/air-quality-data/>.

NASA's A-train Satellite Retrievals

MODIS Thermal Anomalies/Fire Product

We use multiple pieces of information on fires and smoke retrieved from NASA's A-train satellite sensors. The MODIS sensors aboard the Terra and Aqua platforms detect fire spots at $1 \times 1 \text{ km}^2$ spatial resolution globally on a daily basis. The fire detection is performed using a contextual algorithm (Giglio *et al.*, 2003, 2016) that exploits the strong emission of mid-infrared radiation from fires. The algorithm consists of a series of spectral tests and classification of each pixel of the MODIS image. Ultimately, it assigns one of the following classes to each pixel: missing data, cloud, water, non-fire, fire, or unknown. After the classification of cloud and water pixels using their respective masks, and also the obvious non-fire pixels, the algorithm performs background characterization using neighboring pixels in a window centered on the potential fire pixel. Following the successful background characterization, a series of contextual threshold tests are performed for the relative fire detection by looking at the characteristic signature

Table 1. Datasets used in this analysis.

Sensor	Dataset Characteristics	Data Period
MetOne BAM-1020, U.S. Embassy, New Delhi, India	Hourly measurements of PM _{2.5} in $\mu\text{g m}^{-3}$	2013–2016
MODIS	Terra & Aqua MODIS C006 5-min Level-2 Thermal Anomalies/Fires Product at 1-km pixel resolution MOD14/MYD14	2002–2016
OMI	Aqua/MODIS Level-2 MAIAC Aerosol Product at 1-km resolution	
CALIOP	OMAERUV Level-2 Aerosol product of UV-AI, AAOD at native pixel resolution of $13 \times 24 \text{ km}^2$	2004–2016
HYSPLIT	Level-2 Aerosol Layer and Profile product at 5-km horizontal resolution	2013–2016
	Back-trajectories using NCEP/GDAS 0.5×0.5 degree resolution dataset	October and November 2013–2016

of an active fire in which both the $4 \mu\text{m}$ brightness temperature and the 4 and $11 \mu\text{m}$ brightness temperature differences depart substantially from that of the non-fire background. Candidate pixels that pass the above tests are assigned a class of fire. A detailed description of the MODIS fire detection algorithm can be found in Giglio *et al.*, (2003, 2016), and in the Algorithm Theoretical Document Basis (ATBD) at URL http://modis-fire.umd.edu/files/atbd_mod14.pdf. For the present study, we accessed the MODIS Thermal Anomalies/Fire 5-Min L2 Swath 1-km data (Collection 006) retrieved from both Terra (MOD14) and Aqua (MYD14) platforms from the NASA Fire Information for Resource Management System (FIRMS) (<https://earthdata.nasa.gov/earth-observation-data/near-real-time/firms>). As described in the MODIS Collection 6 Fire user guide (https://cdn.earthdata.nasa.gov/conduit/upload/3865/MODIS_C6_Fire_User_Guide_A.pdf), each fire pixel detected by the thermal anomalies algorithm at 1-km resolution is assigned to one of the three confidence classes (low, nominal, or high) depending on its calculated confidence value (C) ($0\% \leq C < 30\%$, $30\% \leq C < 80\%$, $80\% \leq C < 100\%$). A confidence level in the detection of fire spot helps users gauge the quality of individual fire pixels. In the present study, we use fire pixel data with confidence value $C > 30$ relating to the confidence class of ‘nominal’ and ‘high’. Both classes assure fewer false detection of fire pixels.

MODIS MAIAC Aerosol Optical Depth

The Multi-Angle Implementation of Atmospheric Correction (MAIAC) algorithm retrieves surface bi-directional reflection factor (BRF) and aerosol optical depth (AOD) using the time series of MODIS measurements over both dark vegetated surfaces and bright targets (Lyapustin *et al.*, 2011). The surface characterization in MAIAC is carried out by deriving the spectral regression coefficients that relate the surface BRF in the blue (470 nm), green (550 nm), and shortwave infrared (2100 nm) bands of MODIS. MAIAC considers two discrete aerosol models, i.e., background and dust, similar to the ones adopted in MODIS dark target algorithm (Levy *et al.*, 2007). For identifying the smoke aerosols generated from biomass

burning, which is the central issue of the present paper, MAIAC employs a “smoke test” to discriminate smoke from clouds (Lyapustin *et al.*, 2012). The smoke test relies on a relative increase of aerosol absorption at MODIS wavelength $0.412 \mu\text{m}$ as compared to 0.47 – $0.67 \mu\text{m}$ due to multiple scattering and enhanced absorption by organic carbon released during biomass burning combustion. This principle of detecting absorbing aerosols through enhanced absorption at the shorter wavelengths has been successfully demonstrated using the near-UV wavelengths of TOMS (Torres *et al.*, 1998) and OMI (Torres *et al.*, 2007). Each valid 1-km AOD retrievals of MAIAC is assigned with the associated quality flag which describes the observed conditions and overall quality of inversion. In the present work, we use the best AOD retrievals of MAIAC with some relaxations on the quality flags to capture the substantial smoke loading conditions over northern India region. A recent validation study of MAIAC AOD retrievals against ground-based Aerosol Robotic Network (AERONET) over IGP region revealed a good level of agreement with over 70% of matchups falling within the expected uncertainty with a correlation of ~ 0.9 and root-mean-square-error of ~ 0.15 (Mhawish *et al.*, submitted). The MAIAC 1-km retrieval dataset is used here to investigate the AOD-PM_{2.5} link and calculate the trend in columnar aerosol loading over the IGP region during the Aqua operation period.

OMI NEAR-UV Aerosol Product (OMAERUV)

The Ozone Monitoring Instrument (OMI) launched in 2004 onboard NASA’s Aura satellite measures the backscattered radiation emanated from Earth in the spectral range 250–500 nm. Though the primary objective of OMI is to derive total column Ozone, OMI observations are also used to detect UV-absorbing aerosols and measure their properties. The UV Aerosol Index (UV-AI) derived from a pair of wavelengths, i.e., 354 nm and 388 nm, from OMI represents the color of a scene in the near-UV when the Rayleigh scattering component is taken out from TOA radiances. The UV-AI deduced from 340–380 nm wavelength pair of TOMS instrument onboard Nimbus-7 platform is shown to be an excellent indicator of the presence of absorbing aerosols such as windblown dust aerosols and

carbonaceous particles generated from biomass burning (Torres *et al.*, 1998). The two-channel near-UV algorithm OMAERUV of OMI also inverts the TOA radiances at 354 and 388 nm and retrieves the total columnar AOD and Single-scattering Albedo (SSA), and Aerosol Absorption Optical Depth ($\text{AAOD} = \text{AOD} \times (1 - \text{SSA})$) at 388 nm at a pixel resolution of $13 \times 24 \text{ km}^2$ (Torres *et al.*, 2007, 2013). OMI retrievals of AOD and SSA have been validated and inter-compared globally against the ground-based direct and inversion measurements made by the ground-based AERONET sunphotometers. The combined OMI-AERONET AOD analysis for major 44 sites yields correlation, slope, and intercept of 0.81, 0.79, and 0.10, respectively, with 65% matchups falling within the uncertainty levels of $\pm 30\%$ (Ahn *et al.*, 2014); whereas an inter-comparison of SSA using inversion data from all AERONET sites showed an agreement within ± 0.03 and ± 0.05 limits for about 50% and 70% of matchups, respectively (Jethva *et al.*, 2014a). Both studies showed that the OMAREUV dataset of AOD and SSA are of sufficient accuracy. In the present study, we use the latest publicly released OMAERUV product (version 1.8.9.1), which includes several major upgrades and provides improved retrievals of aerosols over the last operational version 1.4.2. The dataset was obtained from NASA's GES-DISC data center.

CALIOP/CALIPSO Aerosol Layer and Profile Products

Cloud-Aerosol Lidar and Infrared Pathfinder Satellite Observations (CALIPSO) is a space-based LIDAR-satellite, launched in 2006, for study the vertical distribution of aerosol and clouds (Winker *et al.*, 2007, Chand *et al.*, 2008). It is a part of NASA's A-Train constellation of satellites for coincident Earth observations and flying just a few minutes away from Aqua/MODIS. Having an active LASER-light source at 532 and 1064 nm, CALIPSO is operational all time in its orbit profiling the atmosphere during the day and night. Here, we use the CALIOP Level-2 aerosol layer and profile products derived from the detailed vertical measurements of backscatter (Young and Vaughan, 2009). The product provides vertical profiles of total attenuated backscatter (532 nm and 1064 nm) and the location of each aerosol layer identified at a 5-km horizontal resolution. A cloud-aerosol discriminator score of -80 to -100 is used to separate the aerosol layers from clouds which provided better confidence in the detection of aerosol layers. All detected aerosol layers with opacity flag ≤ 1 are considered in this analysis. We use four years (2013–2016) of CALIOP data of aerosol layers observations corresponding to the post-monsoon season over the crop burning region (29°N – 32°N , 74°E – 77°E).

NOAA'S Hysplit Back-trajectory Data

The back-trajectory data was obtained from the Hybrid Single-Particle Lagrangian Integrated Trajectory model (HYSPLIT), developed by NOAA's Air Resources Laboratory (Stein *et al.*, 2015). It is one of the most widely used models for the atmospheric trajectory and dispersion calculations. The calculation of trajectories in HYSPLIT is performed using averages of the three-dimensional velocity

vector at their initial and first-guess position. Only the advection component is considered when running trajectories. HYSPLIT calculates backward-in-time advection coupled with dispersion by applying the dispersion equations to the upwind trajectory calculation. Coupling the back-trajectory calculation with a Lagrangian dispersion component can produce a more realistic depiction of the link between the concentrations at the receptor and the sources influencing it. Two primary sources of uncertainties that can creep into the back-trajectory calculations are the errors in prescribing initial conditions also called "meteorological grid" ensemble, and model parameterization called the "turbulence" ensemble. While the former ensemble is created by slightly offsetting the meteorological data to test the sensitivity of the advection calculation to the gradients in the meteorological data fields, the latter represents the uncertainty in the concentration calculation resulting from the model's characterization of the random motions created by atmospheric turbulence (Stein *et al.*, 2007). We ran the HYSPLIT model online using the Real-time Environmental Applications and Display sYstem or READY (Rolph, 2017; <http://www.ready.noaa.gov>) and NCEP/GDAS global data at $0.5^\circ \times 0.5^\circ$ resolution (Kanamitsu *et al.*, 1989) to calculate the backward-in-time trajectories.

RESULTS

Temporal Evolution of Fires, Associated Smoke Parameters, and $\text{PM}_{2.5}$

Fig. 2 shows the 4-year long time-series (2013–2016) of 7-day running averaged (a) thermal anomalies or fire counts detected by Terra and Aqua MODIS over Punjab, India and surrounding region (Longitude 74°E – 77°E ; Latitude 29°N – 32°N), (b) the UV-AI and AAOD retrieved by Aura/OMI, (c) AOD (470 nm) derived from Aqua/MODIS MAIAC algorithm, and (d) $\text{PM}_{2.5}$ mass concentration measured downwind of the fire region and at the U.S. Embassy site in New Delhi. The data shown as thick colored lines correspond to October and November for each year, whereas those in gray represent other months. The purpose of this analysis was to co-analyze the temporal evolution of crop fires and resulting aerosol parameters simultaneously. The time-series of fire counts reveals two distinct fire seasons over the region; the one in the post-monsoon season associated with the rice residue burning peaking during the later/early part of October/November, and another in May associated with the wheat residue burning. Compared to the rice stubble burning in post-monsoon, fire counts detected during May are significantly lower in numbers by a factor of 6 to 8. As a result, the emissions of particulate matter and gaseous pollutants are also relatively lower (Badrinath *et al.*, 2006) in May. The impact of crop residue burning during wheat harvesting period (April–May) on air quality has not been investigated in this paper and deserves a separate analysis.

Noticeably, the time-series of fire counts show that Aqua/MODIS (afternoon overpass around 1:30 PM equator-crossing local time) detects significantly more fires, by a factor of 4–5, than those identified by Terra/MODIS (morning overpass around 10:30 AM equator-crossing local time). A

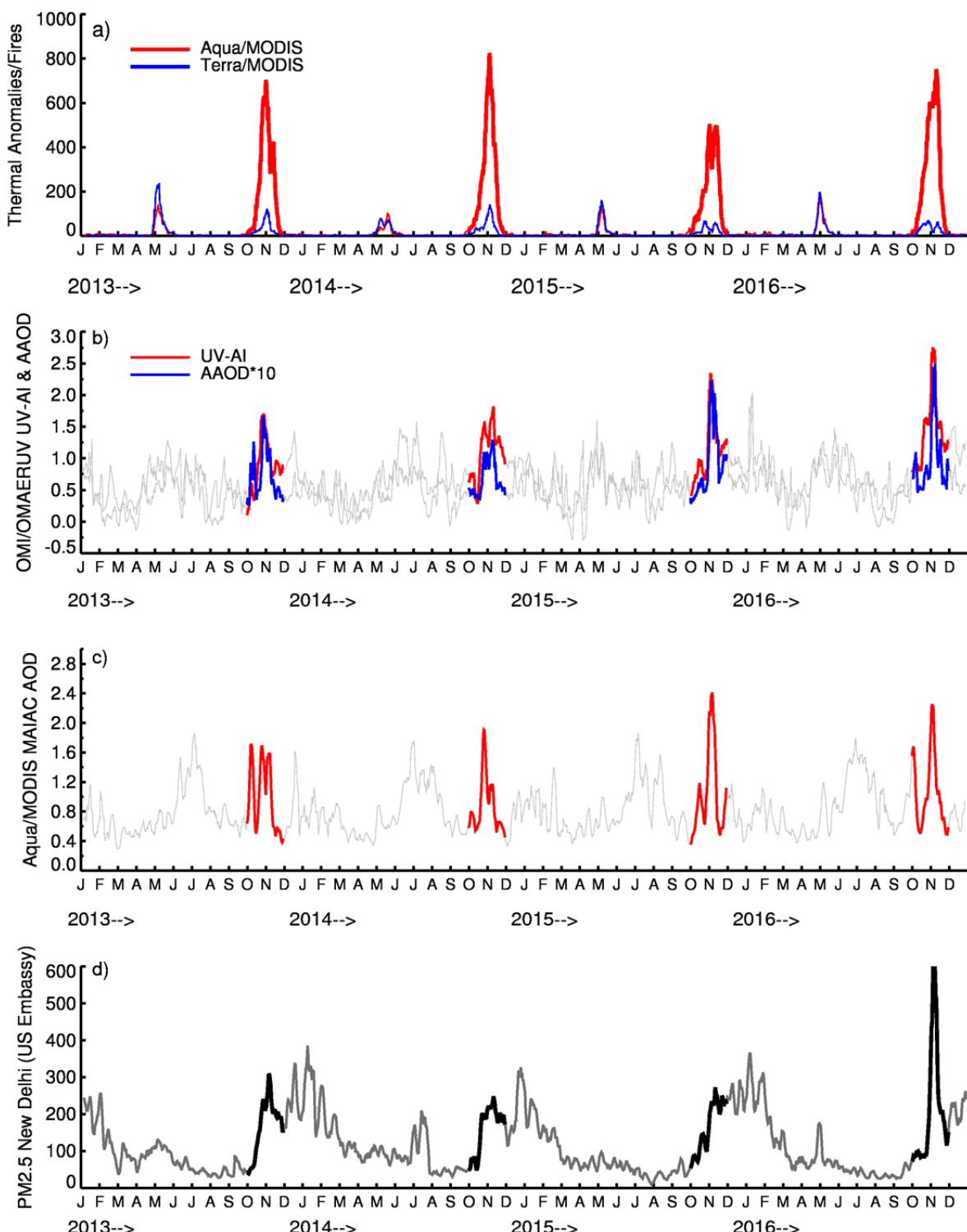


Fig. 2. Time-series showing 7-day running mean of (a) Terra-Aqua/MODIS Collection 006 fire counts, (b) OMAERUV UV-AI and AAOD (388 nm), (c) Aqua/MODIS MAIAC AOD (470 nm); all three correspond to the agricultural fire region (Longitude: 74°E–77°E; Latitude: 29°N–32°N) of Punjab, and (d) PM_{2.5} measured at the U.S. Embassy site in New Delhi. Data shown in thick, bold color represent the months of October and November.

visual analysis of the true-color RGB images overlaid with the fire spots on NASA's Worldview visualization tool (<https://worldview.earthdata.nasa.gov/>) also confirms that the fires and associated smoke loading over Punjab are

drastically higher in Aqua/MODIS data than those observed in Terra/MODIS images. The morning/afternoon cloud cover doesn't seem to be a responsible factor leading to the observed differences in the fire counts between the Terra

and Aqua platforms. We have also looked at the contemporary (2002–2016) time-series of fire counts from both Terra and Aqua (not shown here) and noticed that Aqua detects a significantly larger number of fire counts than those from Terra throughout the 15-year long record. The morning/afternoon asymmetry in fire counts indicates that farmers tend to burn the most amounts of crop residue in the afternoon hours before the Aqua overpasses the region around 1:30 PM local time.

The UV-AI and AAOD, both are strong indicators of the presence of light-absorbing aerosols, derived by OMI along with the time-series of AOD from MODIS-MAIAC product show distinct peaks during post-monsoon coinciding with the peaks in fires over the region. The mass concentration of $\text{PM}_{2.5}$ measured at the downwind location at the U.S. Embassy site in New Delhi also shows a coherent increase, rising in the beginning of October and sharply reaches to a peak value close to $\sim 300 \mu\text{g m}^{-3}$ (24 hour averaged, 7-day running average) at the beginning of November when the fire counts also peak. During the crop burning season of 2016, the 7-day running mean $\text{PM}_{2.5}$ peaked at the record high level at about $550 \mu\text{g m}^{-3}$.

A bar chart of the statistical analysis of $\text{PM}_{2.5}$ measured at the U.S. Embassy site is shown in Fig. 3. Top panel (a) shows the number of days in a month with daily averaged $\text{PM}_{2.5}$ exceeding the annual mean concentration (116, 131, 108, and 123 $\mu\text{g m}^{-3}$ for the year 2013, 2014, 2015 and 2016, respectively) for the four years under consideration. The National Ambient Air Quality Standards of India (http://cpcb.nic.in/National_Ambient_Air_Quality_Standards.php) adopts the limits of $60 \mu\text{g m}^{-3}$ and $40 \mu\text{g m}^{-3}$ as its standards for the 24-hour averaged and annual mean mass concentration in $\text{PM}_{2.5}$, respectively. Compared to the $\text{PM}_{2.5}$ national air quality standards in the U.S.A (<https://www.epa.gov/criteria-air-pollutants/naaqs-table>), the standard of $\text{PM}_{2.5}$ in India is already higher by a factor of about 2 for the 24-hour averaged limit ($35 \mu\text{g m}^{-3}$ in the U.S.A versus $60 \mu\text{g m}^{-3}$ in India) and by a factor of 3 for the annual mean ($12.5 \mu\text{g m}^{-3}$ in the U.S.A versus $40 \mu\text{g m}^{-3}$ in India). The annual mean concentration of $\text{PM}_{2.5}$ measured at the U.S. Embassy site in New Delhi for the last four years is higher by a factor of about two compared to the annual mean standard set by the Central Pollution Control Board in India. When combined, October and November together have a total of 158 (65%) days out of the total 244 days for with the 24-hour averaged $\text{PM}_{2.5}$ exceeding the equivalent national standard of $60 \mu\text{g m}^{-3}$. This is higher by a factor of 2 than the total number of exceedance days (70) from March through September. During winter (December, January, February), about 82% (298 days) of the total number of days (361) exceeded the national standard. Also, it is worthwhile to note that excluding $\text{PM}_{2.5}$ data for October and November brings down the annual mean concentration of $\text{PM}_{2.5}$ by 10%, 7%, 12%, and 13% for the year 2013, 2014, 2015, and 2016, respectively.

In the bottom panel of Fig. 3(b), a time-series of monthly anomalies (%) in $\text{PM}_{2.5}$ calculated for each month with respect to the four-year averaged value ($119 \mu\text{g m}^{-3}$) explains that the percent anomaly for October was $\sim \pm 10\%$, it was

as high as 70–150% for November when the fire activities are at peak (Fig. 2). Besides the post-monsoon months, the anomaly was also noted higher for the winter months of December, January, and February, leaving all other months showing negative anomalies with varying magnitudes. Fig. 3 brings out an important observation about the seasonal variability of $\text{PM}_{2.5}$ in which the higher levels of $\text{PM}_{2.5}$ measured during post-monsoon and winter months contribute the maximum in elevating the level of annual-averaged mass concentration of fine size particles. The wintertime high $\text{PM}_{2.5}$ values are associated with pollution favorable weather conditions (i.e., low temperature, shallow boundary layer, stable atmospheric conditions with calm winds) accompanied with vehicular and industrial emissions and enhanced domestic burning (Girolamo *et al.*, 2004).

Correlation Analysis of Ground-level $\text{PM}_{2.5}$, Satellite Fire Counts, and Aerosol Retrievals

Transport of smoke particles from the source to the receptor region is a continuous process mainly governed by the wind direction and speed, the altitude at which the transport occurs, dispersion and removal along the transport path. To explore the relationship between the satellite observations over the source locations and the $\text{PM}_{2.5}$ at the receptor site in New Delhi, an appropriate time window is required that adequately accounts for the above-mentioned meteorological effects. To determine an optimum time window, we carried out the back-trajectory analysis using the HYSPLIT online tool for the crop burning months (October and November) of 2015 and 2016. Back-trajectories were calculated for each day of October and November of both years at three altitudes, i.e., 100 m, 500 m, and 1500 m, starting at 1:30 PM local time in New Delhi. The back-trajectory data were then used to calculate the averaged time (in hours) taken by the airmass to travel from three representative locations in Punjab covering the northwest-southeast extent of the crop burning area to over a fixed location in New Delhi. As shown in Table 2, the averaged time taken by airmass to arrive at the receptor site depends on its location over the crop fires region and on the altitude of trajectory. Due to its proximity to the receptor site in New Delhi, trajectories passing over the eastern Punjab location (a distance of ~ 185 km from New Delhi) take the shortest time to arrive in New Delhi compared to the time taken from the other two locations. Trajectories intercepting the western Punjab location require the longest time (51, 42, and 24 hours at 100, 500, and 1500 m). Based on this analysis, we select a three-day time window (including the day in consideration) over which the satellite retrievals and $\text{PM}_{2.5}$ measured at New Delhi should be temporally averaged. The three-day window, i.e., a day in consideration and two days prior to it, encompasses the shortest (15 hours) to longest (51 hours) time window that the airmass at all three altitudes would take to mobilize from the crop burning region to over New Delhi. It is expected that the co-location procedure adopted here will resolve some of the variabilities in meteorological fields and transport pattern and facilitate the comparison of the quantities measured independently over the two adjacent regions.

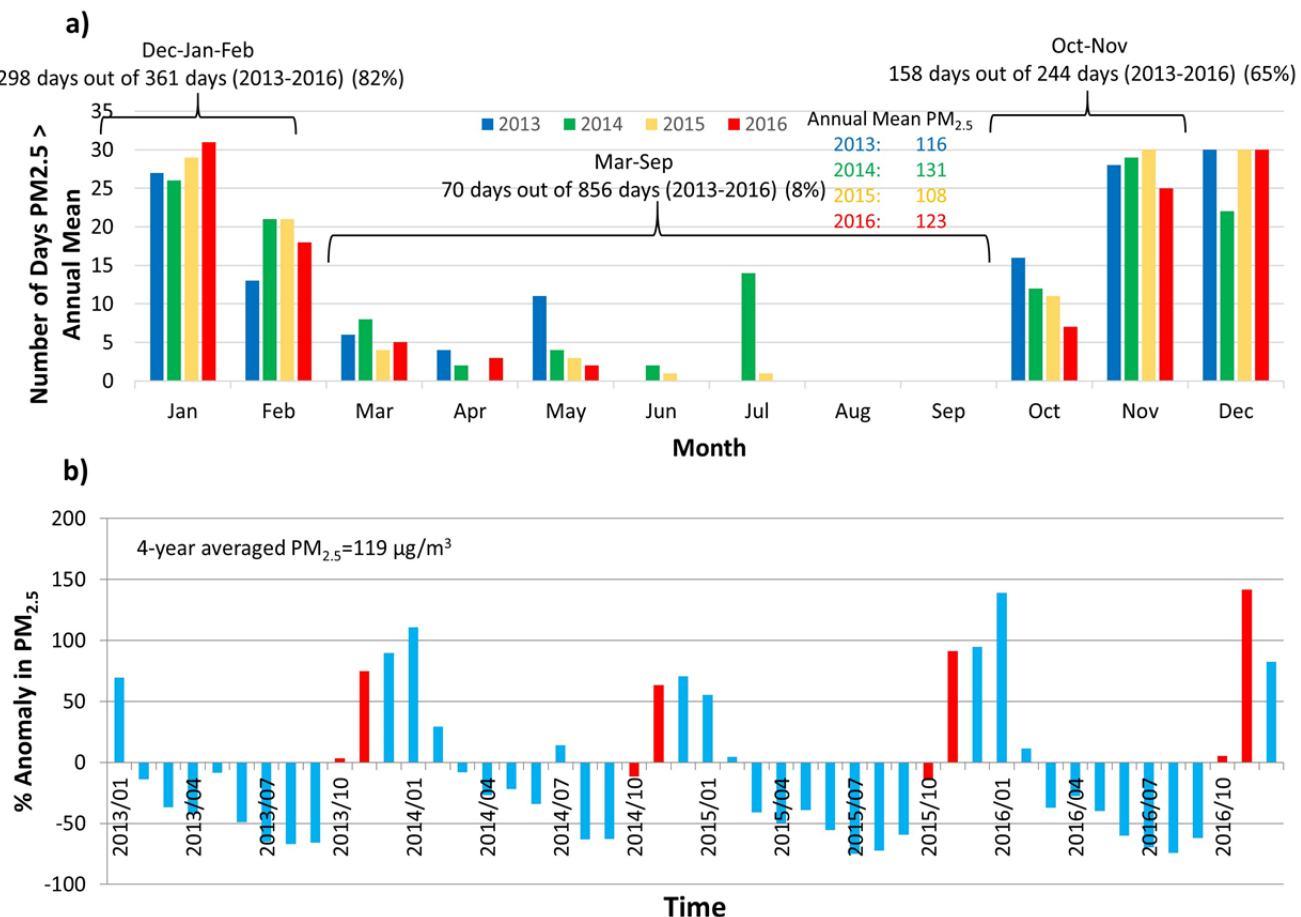


Fig. 3. (a) Bar chart of the number of days in each month with PM_{2.5} exceeding annual mean concentration in the respective years (2013–2016); (b) time-series of % monthly anomaly in PM_{2.5} with respect to the 4-year averaged value (119 $\mu\text{g m}^{-3}$) measured at the U.S. Embassy site in New Delhi; data for October and November are shown in red, whereas those of other months are shown in blue.

Table 2. Time (in hours) taken by trajectories that intercept the crop burning locations in Punjab, India along the transport pathways ending at the receptor location in New Delhi (77.2°E–28.58°N).

Approximate Distance from New Delhi (in km)	Time taken by trajectories ending at New Delhi		
	100 m	500 m	1500 m
Eastern Punjab (76E–30N)	185	26 hours	21 hours
Central Punjab (75.50E–30.75N)	275	35 hours	25 hours
Western Punjab (74.60E–31.75N)	420	51 hours	42 hours

Fig. 4 shows the plots of PM_{2.5} measured at the U.S. Embassy site in New Delhi versus (a) Aqua/MODIS detected fire counts, (b) Aqua/MODIS MAIAC-retrieved AOD (470 nm), (c) UV-AI and (d) AAOD, latter two retrieved from OMI using the two-channel OMAERUV algorithm. The relationships are shown as the standard box and whisker plot, where the dash and filled circles represent the median and mean values for each bin respectively, the thick vertical bars show the range of data in the 25 percentile (median value of the lower group) to 75 percentile (median value of upper group), and thin vertical lines represent the data that falls within 1.5 times the inter-quartile range (75 quartiles minus 25 quartiles). These quantities were calculated for

those bins where the corresponding number of samples exceeds 5; otherwise only mean values were computed and displayed.

We found a well-defined relationship between fire counts, AOD, UV-AI, and AAOD averaged over the upwind region and PM_{2.5} measured in New Delhi. It was noticed that Aqua/MODIS did not detect enough fires over Punjab and Haryana towards the end of the burning season, i.e., last 7 to 10 days of November in all four years. This could be likely due to diminishing fires and also because of smaller spatial scales of the remaining fires missed by MODIS at its 1-km grid resolution at nadir. MODIS true-color RGB images, on the other hand, showed persistent haze over the

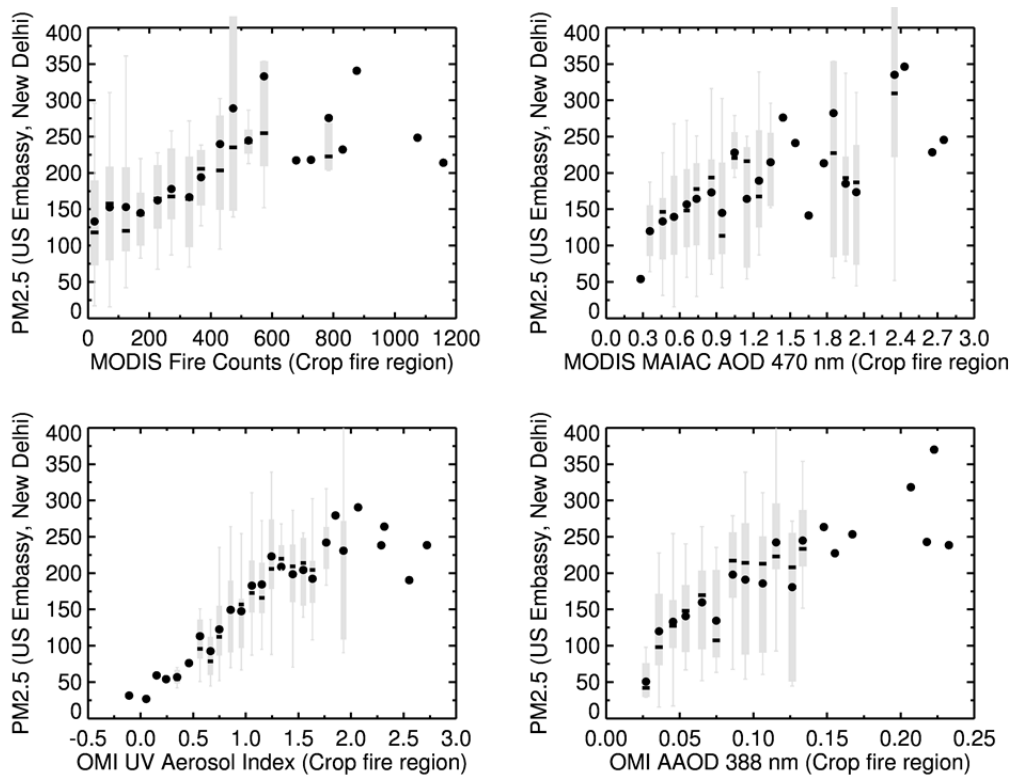


Fig. 4. Relationships of $\text{PM}_{2.5}$ measured at the U.S. Embassy site in New Delhi versus (a) Aqua/MODIS fire counts, (b) Aqua/MODIS MAIAC AOD (470 nm), (c) Aura/OMI-derived UV Aerosol Index, and (d) Aura/OMI-retrieved AAOD (388 nm). Data are represented as standard Box and Whisker plot with dark filled circles as the median value of $\text{PM}_{2.5}$, thick vertical bars represent the 75 (top) and 25 percentiles (bottom) of the samples, and thin vertical bars in gray are the 1.5 times inter-quartile range (75–25 percentile).

region and also a ground-based sensor at New Delhi measured the higher concentration of $\text{PM}_{2.5}$ ($> 150 \mu\text{g m}^{-3}$) during these days. This resulted in a considerable spread in the $\text{PM}_{2.5}$ data at lower fire counts. Overall, the fire counts (up to 600) and $\text{PM}_{2.5}$ showed almost a linear relationship, which yields an increase in $\text{PM}_{2.5}$ of about $33 \mu\text{g m}^{-3}$ given increment in fire counts by about 100. After that, an increase in the numbers of fires (> 600 counts) seems to lose its correlation with $\text{PM}_{2.5}$ where the latter remained in the range 200 – $250 \mu\text{g m}^{-3}$.

Table 3 lists the regression parameters of the $\text{PM}_{2.5}$ versus satellite measurement relationships calculated based on their mean values. The 'All Data' group includes data points from the entire range of measurements, whereas the 'Restricted Data' group considers the range of measurements in which the relationship appears to be near-linear. In all four satellite parameters, the 'All Data' yields larger root-mean-square-error and lower correlation compared to the ones calculated using 'Restricted Data' group, suggesting that the relationship between satellite data and $\text{PM}_{2.5}$ is non-linear when the entire range of observations was considered. In the 'Restricted Data' group, the MODIS fire counts and OMI UV-AI provided the lowest fitting error of $29 \mu\text{g m}^{-3}$ and $19 \mu\text{g m}^{-3}$, respectively. Also, the UV-AI-AAOD- $\text{PM}_{2.5}$ relations yield lowest values intercepts that are closer to the background $\text{PM}_{2.5}$ concentration of $\sim 50 \mu\text{g m}^{-3}$ (7-day running mean) measured by the ground instrument prior to the

onset of burning at the beginning of October (see Fig. 2(d)). The relationships obtained using the 'Restricted Data' group revealed the slope values as ~ 0.33 , 65 , 120 , and 2190 between the $\text{PM}_{2.5}$ and fire counts, MODIS AOD, OMI UV-AI, and OMI AAOD, respectively. In other words, the slope values translate into an overall rate of increase in the mean value of $\text{PM}_{2.5}$ by ~ 33 , 65 , 120 , and $219 \mu\text{g m}^{-3}$ given the increments of 100 , 1.0 , 1.0 , and 0.1 in fire counts, AOD, UV-AI, and AAOD, respectively.

Vertical Structure of Smoke Aerosols

Owing to its lower temporal and spatial coverage, a co-analysis of CALIOP data with other A-train sensors renders very limited statistics of the overlapped datasets. Therefore, the CALIOP lidar data on the vertical distribution of aerosol layers over the crop burning region and over New Delhi (Fig. 5) are studied independently regardless its collocation with other A-train sensors. The main purpose of using CALIOP data here is to locate the prevalent altitudes at which the aerosol layers reside and examine the detailed vertical profiles over the study area. Fig. 5 shows the histograms of the altitude-dependent number of aerosol layers detected by the CALIOP during daytime (a) and nighttime overpasses (b) over the crop-residue burning region of Punjab and Haryana for the post-monsoon months of October and November of years 2013–2016. Owing to its better signal-to-noise ratio, CALIOP detects a larger number

Table 3. Parameters of the linear regression fits between PM_{2.5} and satellite measurements.

	Slope	Intercept	Correlation R ²	Fitting Error	Number of Bins
MODIS Fire Counts	0.15/0.33*	145.63/100.06*	0.46/0.82*	58/29*	20/12*
MODIS-MAIAC AOD (470 nm)	101.49/65.38*	77.16/103.45*	0.39/0.43*	96/43*	25/19*
OMI UV-AI	133.07/119.7*	24.58/33.508*	0.66/0.94*	84/19*	29/22*
OMI AAOD (388 nm)	1813.0/2190.3*	23.39/-5.2692*	0.60/0.69*	107/79*	24/18*

Restricted Data*

Fire Counts < 600; MODIS AOD < 1.5; OMI UV-AI < 2.0; AAOD < 0.20.

Fitting error ($\mu\text{g m}^{-3}$) is defined as the square-root of the averaged square of differences between the actual and regression values of PM_{2.5}.

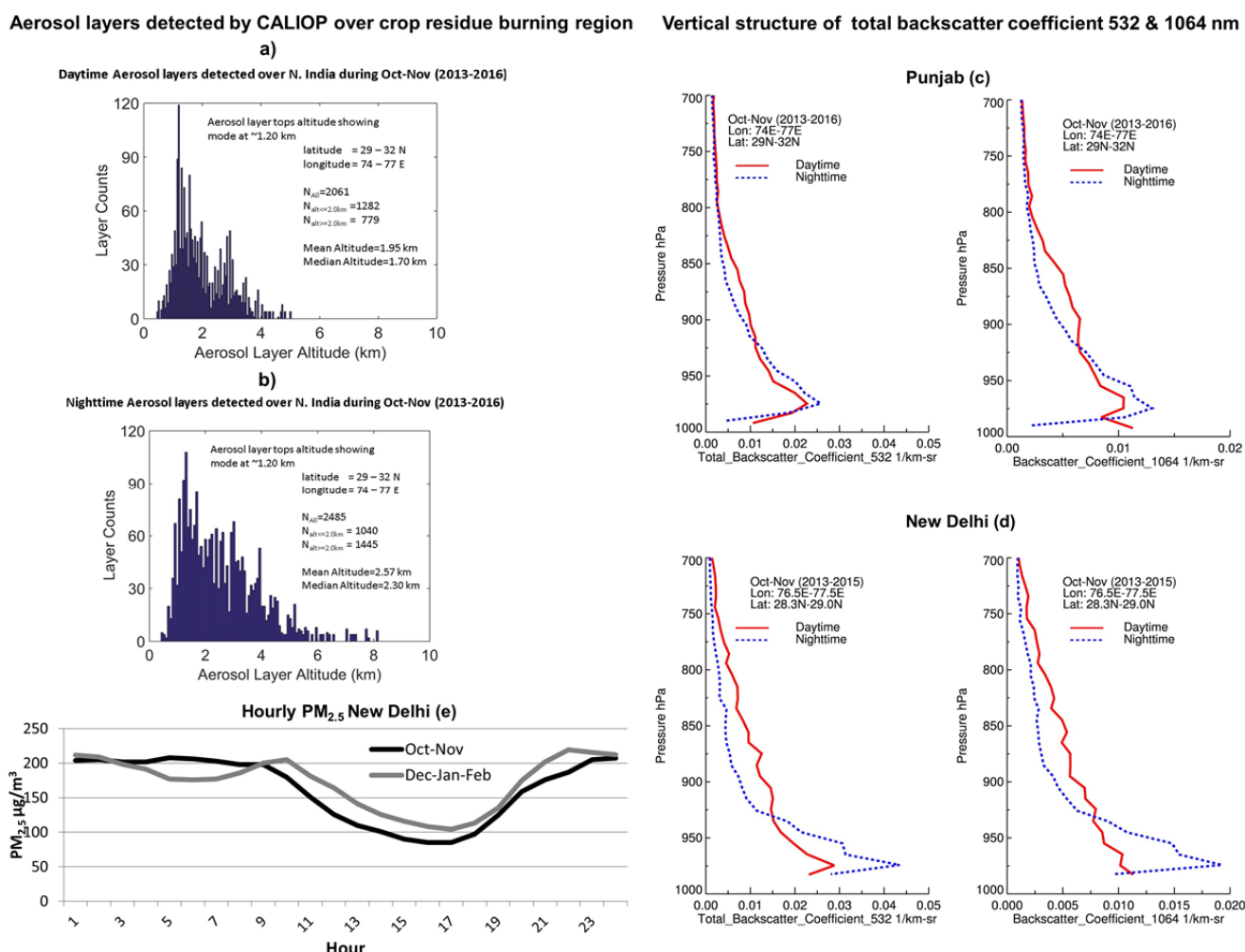


Fig. 5. Histograms of altitude-dependent aerosol layer counts detected by CALIOP lidar during (a) daytime and (b) nighttime over the crop-residue burning region of Punjab during the post-monsoon months of October and November of years 2013–2016. On the right, the averaged daytime and nighttime vertical profiles of total backscatter coefficients for the 532-nm and 1064-nm derived from CALIOP are shown for the (c) Punjab-Haryana region and (d) New Delhi. The hourly-averaged PM_{2.5} measured at the U.S. Embassy site in New Delhi for the post-monsoon (October and November) and winter (December–January–February) months are shown in the bottom panel (e).

of aerosol layers during nighttime (~20%) compared to that during the daytime. While the distribution of aerosol layer top altitudes shows a mode around 1.2 km during both daytime and nighttime observations, the number of layers detected above 2.0 km during nighttime is considerably

higher than that during the daytime. These differences can be attributed to the better signal-to-noise ratio during nighttime than that during daytime, allowing CALIOP lidar to detect aerosol layers with lesser backscatter intensity. Overall, 62% and 42% of the total number of layers are

identified below 2.0 km during daytime and nighttime, respectively, which relate to $\text{PM}_{2.5}$ at the surface.

The average vertical structure of the total backscatter coefficient at 532 nm and 1064 nm derived using daytime and nighttime aerosol observations over the crop residue burning region of Punjab and Haryana (c) shown on the right of Fig. 5 reveals peaks in aerosol backscatter just above the surface and around 975 hPa (~250 m above the ground). Then after, the 532-nm profile (1064- nm profile) approximately follows an exponential distribution with the scale heights of ~1.0 km and ~0.5 km (~1.5 km and ~0.75 km) for daytime (nighttime) observations. For the downwind NCR region, including New Delhi (d), the average vertical structure exhibits similar behavior albeit with the larger magnitudes of peaks near the surface. Noticeably, the vertical profile derived using nighttime observations (around 2:30 AM local time) shows larger values of total backscatter coefficient at both wavelengths, with a pronounced effect at 1064 nm at lower atmospheric levels (> 925 hPa) than those derived from the daytime observations (around 2 PM local time) suggesting a higher concentration of particulate matter near the surface during nighttime overpass than that during daytime overpass. Quantitatively, the peak value of the backscatter coefficient at 532 nm (1064 nm) for the nighttime observations is about 51% (90%) larger than that measured during the daytime. On the other hand, the nighttime coincident observations of mass concentration of $\text{PM}_{2.5}$ (averaged) at the U.S. Embassy around the CALIPSO overpass time shown in Fig. 5(e) is found to be about 100% larger than the daytime coincident observations of $\text{PM}_{2.5}$. When comparing the daytime and nighttime measurements of mass concentration of $\text{PM}_{2.5}$ in New Delhi for the individual days in October and November, it was noticed that the averaged nighttime $\text{PM}_{2.5}$ (9 P.M. to 9 A.M. local time) is higher by 50% to 80% than that measured during daytime (9 A.M. to 9 P.M. local time). In this regard, the 1064-nm backscatter signal of CALIOP provides a better consistency with the independent measurements of $\text{PM}_{2.5}$ regarding daytime versus nighttime variations of aerosol particles over New Delhi.

The CALIOP aerosol-cloud layer detection algorithm uses the 532-nm backscatter measurements to detect discrete layers of aerosols and clouds. Under heavy smoke aerosol loading condition, the 532-nm backscatter signal attenuates rapidly along the transmission path leading to a reduced signal-to-noise ratio for the aerosol layers beneath the strongly attenuated layers. Also, the required correction for the attenuation becomes large resulting in the increased uncertainties in retrievals of the lower layers (Winker *et al.*, 2009). The absence of aerosol layers near the surface in Figs. 5(a) and 5(b) could be attributed to this geophysical feature of the lidar signal. On the other hand, the 1064-nm signal penetrates deeper into the aerosol layers owing to lower aerosol extinction at this wavelength providing a more realistic vertical structure of aerosols (Torres *et al.*, 2013; Jethva *et al.*, 2014b). A supplementary Fig. 1 compares the nighttime Level 1 total attenuated backscatter signal measured at 532 nm and 1064 nm of a case study (November 10, 2015) with heavy smoke aerosol loading over northwestern

India.

Back-trajectory Analysis

Fig. 6 shows the clusters of 3-day (72 hours) back-trajectories calculated using the HYSPLIT model over northern India. Back-trajectories were calculated for each day of October and November of 2013–2016 at three altitudes, i.e., 100 m (a), 500 m (b), and 1500 m (c), starting at 1:30 PM local time in New Delhi. In order for the ground sensor in New Delhi to sample the smoke particles emitted over the crop burning areas, the transport must occur over the first few hundred meters of the atmosphere. Therefore, we choose three altitudes for the back-trajectory analysis, i.e., two closer to the ground (100 m and 500 m) that relate to the $\text{PM}_{2.5}$ and one near the free troposphere boundary at 1500 m for comparison. All trajectories of October and November (a total of 244) are grouped according to the concurrent 24-hour averaged $\text{PM}_{2.5}$ (shown as the legends on the top of Fig. 6) measured at the US Embassy site in New Delhi. This allows us to attribute the variations in $\text{PM}_{2.5}$ at the receptor location to the source regions via transport mechanism. Fig. 6 shows that most trajectories at the near-surface level (100 m), quantitatively, 52%, 81%, 89%, and 84%, corresponding to the respective range of $\text{PM}_{2.5} (\mu\text{g m}^{-3})$, i.e., $0 < \text{PM}_{2.5} < 100$, $100 < \text{PM}_{2.5} < 200$, $200 < \text{PM}_{2.5} < 300$, and $\text{PM}_{2.5} > 300$, intersected the crop burning region of Punjab and Haryana (depicted as a box in the figure) partially or fully before arriving at the receptor location in New Delhi. The corresponding percentages of all back-trajectories for the 500 m altitude were 50%, 89%, 86%, and 84%. Noticeably, over 80% of all trajectories at both altitudes that intersected the crop burning areas are associated with higher level of $\text{PM}_{2.5}$. In other words, days with extreme levels of $\text{PM}_{2.5}$ were associated with the northwesterly flow from the burning areas, suggesting a profound impact of smoke transport on modulating the air quality over New Delhi. Fig. 6 (bottom, d) displays the averaged altitude dependence of the trajectory path as a function of time. Averaging was performed on the hourly data using all trajectories. The averaged trajectories for the altitudes 100 m and 500 nm showed marked subsidence of smoke-laden airmass along the transport pathways indicating downward movement of particulate pollution to the lower levels of the atmosphere thus increasing the concentration of particles at the surface over the receptor location.

An analysis of back-trajectories calculated for several individual days reveals that the transport of smoke produced from agricultural fires typically takes less than a day (~14–22 hours) to be mobilized from the central areas of burning in Punjab to the receptor location in New Delhi. Since the paddy residue burning is widespread throughout the state, the actual time required for the mobilization of smoke particles depends duly on the distance between the fire locations and receptor and wind speed. Assuming the wind speed of 5 m s^{-1} of the northwesterly flow at the lower levels of the atmosphere (> 850 hPa), the transport of smoke would take about 8, 15, and 22 hours to travel from the nearest (~150 km), central (~270 km), and the farthest (~400 km) areas of burning, respectively, to over the NCR.

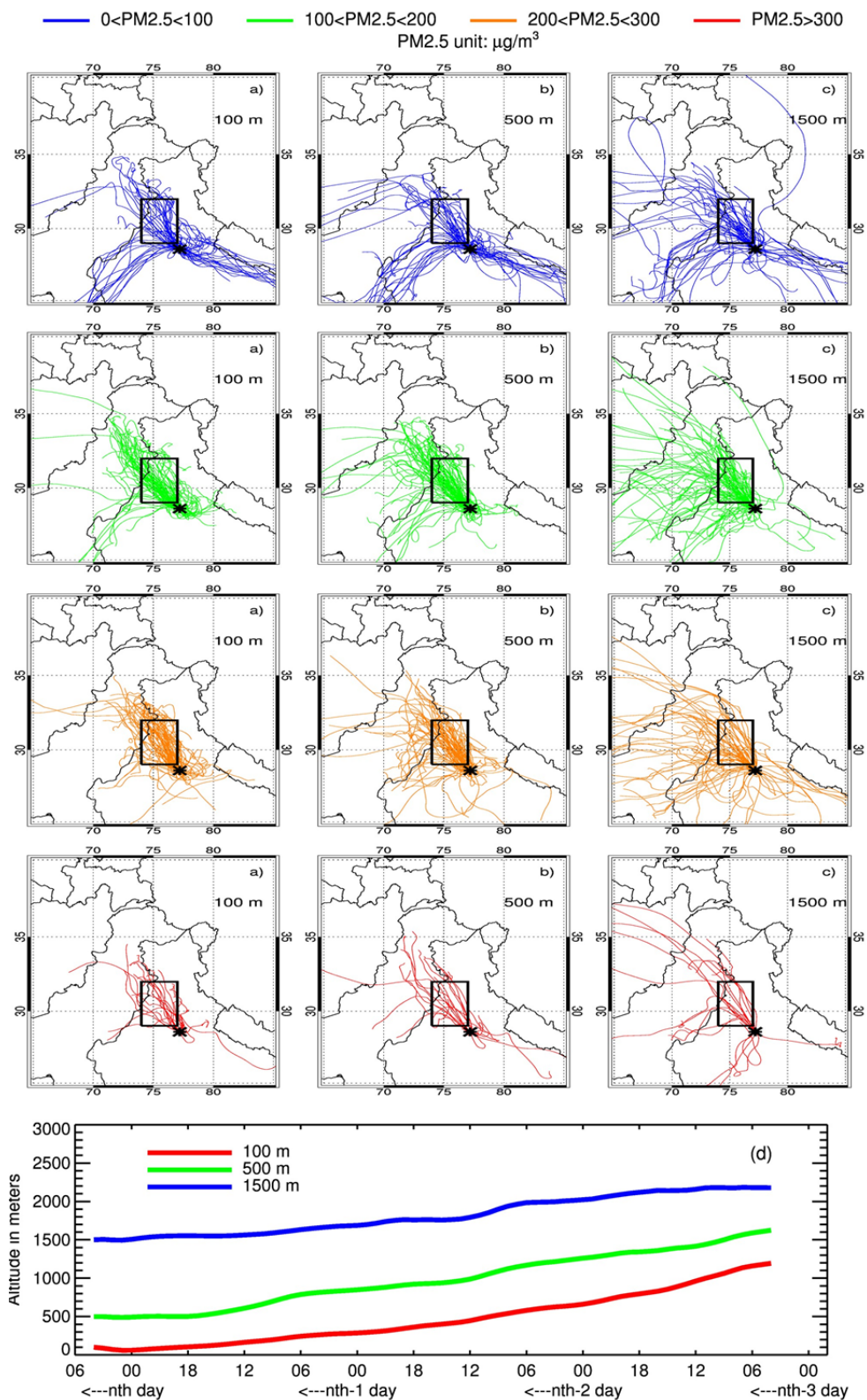


Fig. 6. Clusters of HYSPLIT 3-day back-trajectories originating in New Delhi, India (marked with an asterisk) in October and November of 2013 to 2016. Back-trajectories were calculated once per day with the starting local time of 1:30 PM and for the three altitudes, i.e., (a) 100 m (near-surface), (b) 500 m, and (c) 1500 m. Discrete color codes assigned to each back-trajectory (shown as legends on the top) represent a corresponding range of 24-hour averaged PM_{2.5} measured at the US Embassy site in New Delhi. The crop burning area of the Indian states of Punjab and Haryana is depicted as a bounding box. The bottom panel (d) shows the averaged altitudinal variations of the back-trajectories as a function of time for the three reference altitudes.

Satellite-based Long-term Record of Fires and Smoke Aerosols

The availability of PM_{2.5} data taken at the U.S. Embassy site in New Delhi at the time of the analysis was limited to the four years, i.e., 2013–2016. Therefore, the correlation analysis relating PM_{2.5} and the satellite data was restricted to these four years only (Fig. 4). However, NASA's A-train satellite observations offer a unique opportunity to simultaneously examine the longer-than-decade record (2004–2016) of the temporal and spatial evolution of agricultural fires and resulting smoke aerosol loading over northern India. In this section, we look at the 13-year simultaneous record of fire counts and columnar amounts of aerosols with a focus on understanding the temporal and spatial evolution of atmospheric composition over the greater IGP region modulated by the post-monsoon residue burning over Punjab and Haryana.

Fig. 7 shows the post-monsoon months climatology maps (2004–2016) of the total fire counts (top-left) and columnar AOD (top-right) derived from Aqua/MODIS, UV-AI (bottom-left), and AAOD (388 nm) (bottom right) derived from Aura/OMI. The climatology was calculated by aggregating the Level 2 retrievals at their native resolution onto the 0.25° by 0.25° spatial grids followed by performing an average over the simultaneous Aqua-Aura operation period 2004–2016. The state of Punjab stands out regarding the density of fires in the entire northern Indian subcontinent with a maximum number of fires counts (> 400) seen in the central areas of the state. The density of fire counts in the surroundings, i.e., Pakistan and central/eastern IGP was 5 to 10 times lesser leaving Punjab the only dominant region with intense agricultural fires. UV-AI and AAOD from OMI also show elevated amounts absorbing aerosols over the areas of agricultural fires. A spatial gradient in UV-AI and AAOD along the IGP region with maximum concentration over the crop-residue burning areas in Punjab to relatively moderate levels over the eastern parts of IGP—a distance of about 1300 km from the source region further signifies the transport of smoke produced by the fires in Punjab under the influence of northwesterly winds. Spatial distribution of MAIAC AOD shows the spatial pattern of aerosols consistent with the OMI aerosol observations.

The temporal evolution of fire events is shown in Fig. 8, where the top panel (a) displays the monthly, accumulated total fire counts over the crop burning area (Longitude: 74°E–77°E, Latitude: 29°N–32°N) derived from Aqua/MODIS record. Data in blue and red colors represent the paddy residue burning months of October and November, respectively, whereas those in gray represent other months of the year. The region, as discussed in section 3.1 (Fig. 2), is characterized by the two major fire seasons with the intense burning of paddy residue during post-monsoon followed by wheat residue burning in spring. In contrast to the springtime burning season, fire counts detected during post-monsoon were 5 to 6 times larger. The time-series also reveals a shift in the distribution of fire occurrence from October to November, where Aqua/MODIS observed significantly larger number fires in October during the first half of the record (2002–2009), after which the majority of

the fires were gradually shifted to November. The total number of fire counts detected in October and November combined (shown as thick black square symbols fitted with a polynomial in Fig. 8) reveals an overall positive trend of ~500 fire counts per year with the increasing number of fires during the second half of the Aqua/MODIS record (2009–2016). With reference to the averaged total fire counts (dashed black color line) calculated using the 15-year long Aqua/MODIS record, the total number of fire counts detected during the second half of the Aqua period is found to be 32% higher than that identified during the first half of the record (2002–2009). The time-series also shows interannual variations in fire counts with distinct peaks in the year 2005, 2007, 2012, 2014, and 2016. The crop burning season of the year 2016 has been the most anomalous in the entire Aqua/MODIS record with a maximum number of fire hot spots (17,804) detected over Punjab-Haryana region. Compared to the averaged fires counts (14,310) detected during previous five years, i.e., 2011–2015, the total fire counts in 2016 was noted higher by 24%. The percent increase in the fire counts for the year 2016 went further up to 44% when compared to the averaged fire counts (12,384) calculated for the period 2002–2015.

When separated by the months of crop burning season, the total fire counts detected during October shows a negative trend of –117 fire counts per year over the period 2002–2016 (Fig. 8(b), left panel). Satellite retrievals of AOD (Fig. 8(c), left panel) and UV-AI (Fig. 8(d), left panel) for the broader IGP region (shown as the shaded area in the inset map) shows negligible positive trends over the respective periods. On the contrary, the total fire counts in November show a marked positive trend of +616 fire counts per year (Fig. 8(b), right panel), which is also associated with the positive trends in MAIAC AOD (+0.031 per year) and OMI UV-AI (+0.04 per year). While all three quantities show positive trends during November, some interannual non-coherent variations remain. This could be attributed to different spatial domains considered for averaging, cloud contamination that affects the detection of fire hotspots and aerosols; retrieval uncertainties; and removal, emission, and transformation of smoke particles along the transport pathways. Despite these inherent factors that can modulate the spatial and temporal evolution of smoke events, consistent positive trends in AOD and UV-AI over the greater IGP region concurrent with the positive trend in fire counts over the Indian states of Punjab and Haryana signify that an increase in the fire activities over northwestern India not just affect the air quality over local burning region but also leads to an increased aerosol loading far downwind the source region.

DISCUSSION AND CONCLUSION

The seasonal crop residue burning over the northwestern states of Punjab and Haryana in India is a major source of pollution over the greater IGP region. The burning of waste material resulted from the harvest of rice crop produces aerosols and trace gases in large quantities, which affects the air quality locally and across the region downwind of the sources. The correlation analysis suggests a strong influence

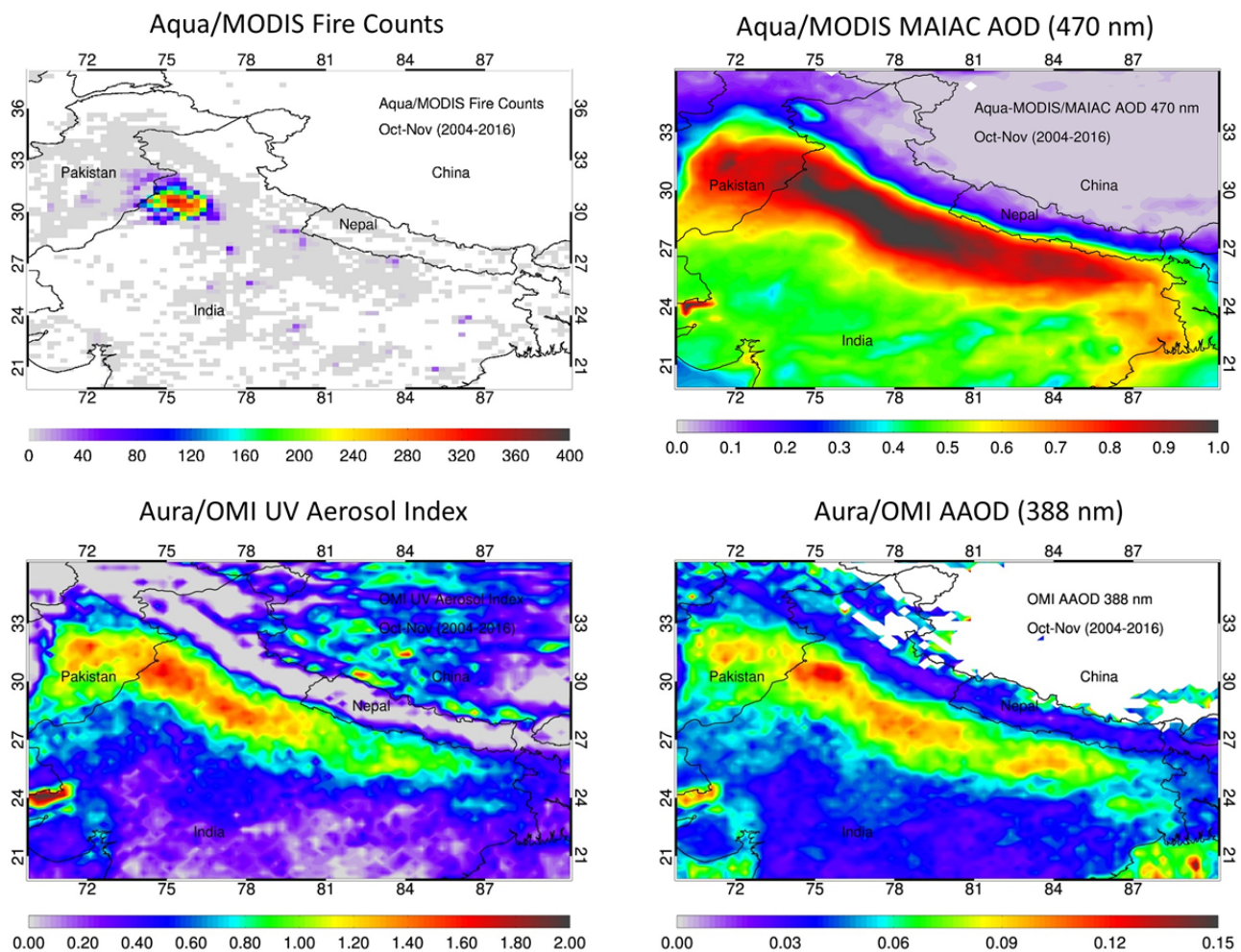


Fig. 7. The 13-year (2004–2016) averaged and gridded (0.25° by 0.25°) maps of total fire counts detected by Aqua/MODIS in October and November (top-left), Aqua/MODIS MAIAC AOD (470 nm, top-right), Aura/OMI UV Aerosol Index (bottom-left), and Aura/OMI AAOD (388 nm, bottom right) over the northern Indian subcontinent.

of crop residue fires and associated smoke aerosols observed by MODIS and OMI sensors over Punjab on the concentration of $\text{PM}_{2.5}$ measured on the ground in New Delhi. However, each relationship renders spread around the central part of the data population. Several factors that could be attributed to the observed dispersion of the data are the following.

First, the correlative analysis compares an area-averaged quantity of the space-based retrievals over Punjab (3° by 3° in longitude and latitude grids) with a ground-level $\text{PM}_{2.5}$ measured at a single location in New Delhi. In this process, it was implicitly assumed that the air mass observed by the A-train sensors over Punjab and surrounding regions is also sampled at the ground location of the U.S. Embassy site in New Delhi, which might not be the case for all data samples. Second, different spatial and temporal scales of transport mechanisms governed by the meteorology, i.e., wind speed, wind direction, boundary layer dynamics, and altitude dependence of transport, can introduce uncertainties in the desired relationship. Third, except for the fire pixels detected by MODIS, the UV-AI and AAOD retrieved by OMI, and AOD by MODIS represent the column properties

of aerosols, whereas $\text{PM}_{2.5}$ measured in New Delhi represents the mass concentration per unit volume at the ground. Therefore, the vertical distribution of smoke particles and variations associated with it along the transport path can affect the relationship. Fourth, the retrievals of fire counts and column aerosol properties are based on the respective inversion algorithms, which rely on a set of assumptions about the properties of the atmosphere and surface. As a result, each of the satellite retrieval datasets used in the present study carries specific uncertainties that can amplify the spread in the relationship between column properties versus ground measurements of particulate matter. Fifth, the temporal collocation procedure considers 3-day averaging of the satellite and ground measurements expecting it to allow adequate time window for the airmass observed by satellites over the fire region to be sampled by the ground sensor in New Delhi. Changes in meteorological fields, including relative humidity, vertical distribution of aerosols, planetary boundary layer height, and vertical mixing are among several other factors that can introduce non-linearities and uncertainties in the satellite-ground measurement comparison. Despite these inherent uncertainties involved

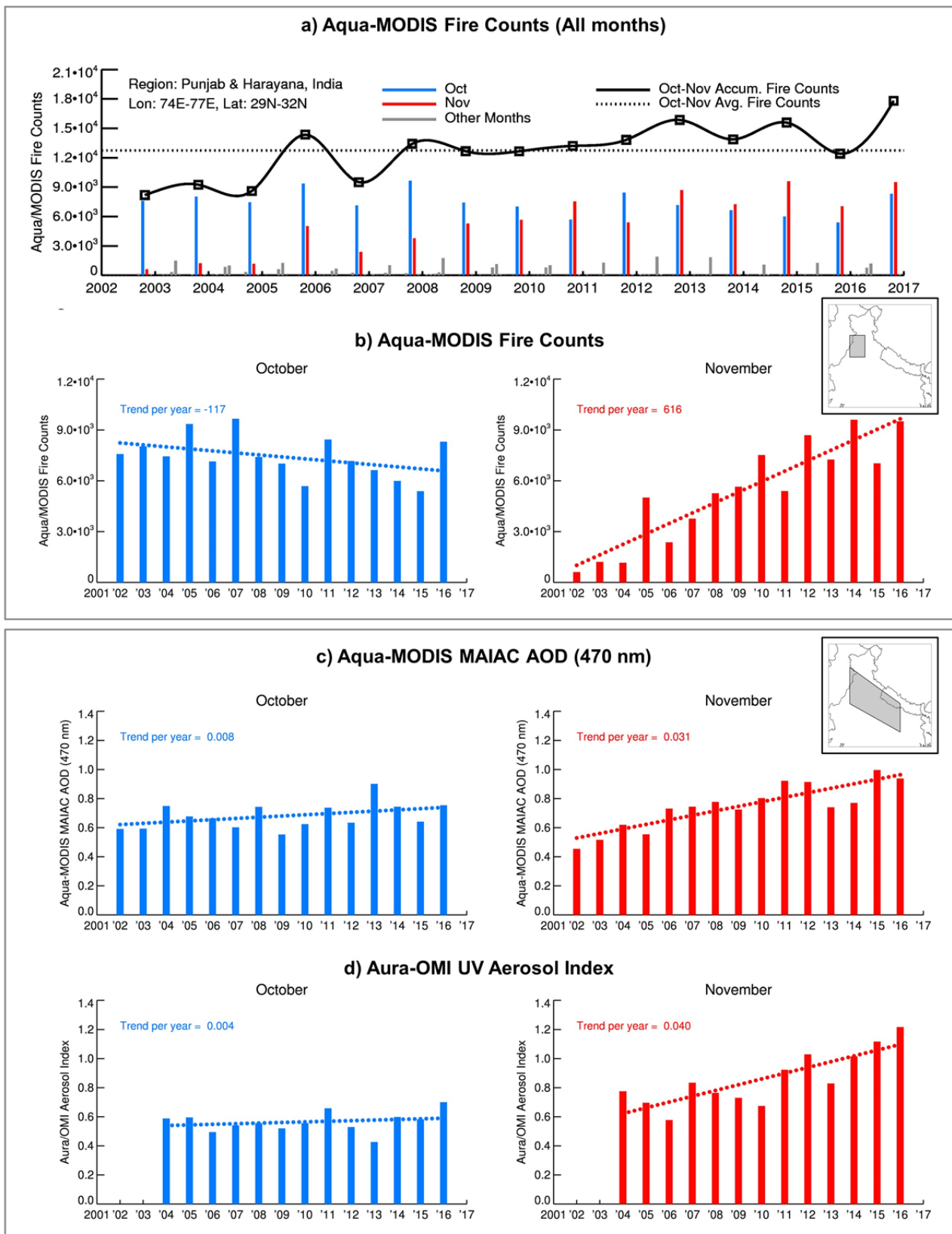


Fig. 8. (Top, a) 15-year time series of accumulated fire counts for individual months (vertical color bars) and accumulated fire counts combined in October and November (black square blocks) detected by Aqua/MODIS over the agricultural burning region of Punjab and Haryana. (b) Monthly time-series of the total number of fire counts for October (left) and November (right), (c) and (d) Monthly time-series of area-averaged MODIS MAIAC AOD at 470 nm and UV-AI, respectively, for October (left) and November (right).

in the methodology, the relationships shown in Fig. 4 has established an unambiguous connection between the satellite measurements of smoke particles over the crop burning region and ground-level concentration of particulate matter downwind, suggesting a strong influence of agricultural fires on the air quality downwind the region via transport mechanism.

Besides the local sources of emissions and transport of pollution from neighboring regions, the meteorology also plays an important role in governing the diurnal variations of PM_{2.5}. The meteorology over northern India during the post-monsoon is characterized by prevailing northwesterly winds with speed generally lower than 5 m s⁻¹, little or no convective activities, the temperature in the range 20–30°C, and relative humidity varies from 40%–70%. The planetary boundary layer (PBL) height, as simulated by Modern Era Retrospective-analysis for Research and Applications 2-D dataset (0.5° × 0.75° spatial resolution) (Badarinath *et al.*, 2010) over the IGP varies between ~300 and ~800 m during post-monsoon. Owing to colder temperature, shallow PBL, and an inversion layer closer to the surface during nighttime, the particulate matter transported from the adjacent region and also produced locally is likely to be confined within the lower atmospheric layers increasing the concentration of PM_{2.5} at the surface. The detailed vertical profile of backscatter signal at 1064 nm measured by CALIOP and PM_{2.5} measured at the ground during daytime and nighttime (see Fig. 5) are found consistent with the diurnal variation of concentration of particulate matter.

Although the present analysis was focused on investigating the impacts of post-monsoon crop fires in Punjab/Haryana over the greater IGP region, including New Delhi, we emphasize here that the emissions of local sources of pollution on the levels of PM_{2.5} within the NCR cannot be ruled out. With a population of about 18 million, vehicle number of approximately 9.5 million, numerous industries, construction activities, and seasonal shift of meteorological patterns from post-monsoon to winter, it is possible that the increase in PM_{2.5} observed during the study period (Figs. 2 and 4) could be partly attributed to the changes in meteorological fields and emissions from the local sources. Assuming near-stable levels of emissions from local sources, i.e., vehicles and industrial pollution during the seasonal transition, the concentration of PM_{2.5} prior to the onset of crop burning (~50 µg m⁻³, 7-day running mean) may be treated as the background level accounting for all the sources of emission other than those from crop fires in Punjab and Haryana. Rising levels of PM_{2.5} past the background concentration, therefore, are most likely attributed to the simultaneous progress in the residue burning in Punjab and Haryana followed by the transport of smoke particles to over New Delhi. Nevertheless, discerning the local contribution from the transported particulate pollution over NCR is still an open question and should be investigated further.

The long-term averages of satellite retrievals shown in Fig. 7 further explain that the impact of crop fires is not just limited to over the source and adjacent areas, but smoke particles travel far from fire hotspots to over the broader IGP region. Increasing number of fire counts over

the crop burning region of Punjab and Haryana during the post-monsoon season and resulting enhancement in the aerosol loading, as shown in Fig. 8, elevates the seriousness of the issue as it affects the air quality in the populous IGP region.

The impact of open field burning of crop stubble on aerosol and gaseous measurements over northwestern India has generally been reported and discussed in several earlier studies (refer to various citations in the Introduction section). However, the present work to our knowledge, brings new information on the crop burning-air quality link as follows.

- 1) The study employs multi-satellite datasets derived from NASA's A-train sensors, including VIS (MODIS), UV (OMI), and LIDAR (CALIOP) instruments offering unique abilities and different perspectives along with the ground-based PM_{2.5} measurements to investigate the impact of seasonal agricultural burning over the northwestern states of India on the air quality over IGP.
- 2) We have developed a quantitative basis of the cause-and-effect relationship between the satellite observations over the burning region and ground measurements of PM_{2.5} downwind in New Delhi, as shown in Fig. 4 and Table 3 in the paper. These relationships are useful for predicting the PM_{2.5}, albeit with some uncertainties, given the satellite measurements in the near-real time.
- 3) By taking advantage of the long-term operation of A-train sensors, we show a 15-year long record of fires and associated aerosol loading over IGP revealing marked positive trends in both geophysical as shown in Fig. 8.

Severely poor air quality during crop fires can have detrimental effects on the health of millions living in IGP—one of the most densely populated regions of the world. Increasing levels of crop residue burning and resulting particulate matter pollution at an alarming rate over northern India is a pressing concern demanding urgent attention and further calls for corrective measures to substantially reduce or completely diminish the crop burning through an effective residue management system.

ACKNOWLEDGMENTS

We thank the support of NCCS data portal, GES-DISC, and ASDC, the NASA Earth Science data centers, for the online availability of the MODIS, OMI, and CALIOP aerosol products used in this analysis. The thermal anomalies/fire spots dataset was obtained from the NASA Fire Information for Resource Management System (FIRMS) (<https://earthdata.nasa.gov/earth-observation-data/near-real-time/firms>). The first author conducted the present work under the Aura/OMI aerosol project grant. Duli Chand acknowledges the support from PNNL operated for DOE by Battelle Memorial Institute under Contract DE-AC06-76RLO1830. We also recognize the Air Quality Monitoring program of the U.S. Department of States and U.S. Embassy, New Delhi for making the PM_{2.5} measurements freely available online. Authors acknowledge the NOAA Air Resources Laboratory (ARL) for the free provision of the HYSPLIT transport and dispersion model and READY online tool (<http://www.ready.noaa.gov>) accessed for simulating the back-trajectories.

SUPPLEMENTARY MATERIAL

Supplementary data associated with this article can be found in the online version at <http://www.aaqr.org>.

REFERENCES

- Ahn, C., Torres, O. and Jethva, H. (2014). Assessment of OMI near-UV aerosol optical depth over land. *J. Geophys. Res. Atmos.* 119: 2457–2473.
- Badarinath, K.V.S., Kiran Chand, T.R. and Krishna Prasad, V. (2006). Agriculture crop residue burning in the Indo-Gangetic Plains - A study using IRS-P6 AWIFS satellite data. *Curr. Sci.* 91: 1085–1089.
- Badarinath, K.V.S., Sharma, A.R., Kaskaoutis, D.G., Kharol, S.K. and Kambezidis, H.D. (2010). Solar dimming over the tropical urban region of Hyderabad, India: Effect of increased cloudiness and increased anthropogenic aerosols. *J. Geophys. Res.* 115: D21208.
- Brauer, M., Freedman, G., Frostad, J., Van Donkelaar, A., Martin, R.V., Dentener, F. and Cohen, A. (2016). Ambient air pollution exposure estimation for the global burden of disease 2013. *Environ. Sci. Technol.* 50: 79–88.
- Chand, D., Anderson, T.L., Wood, R., Charlson, R.J., Hu, Y., Liu, Z. and Vaughan, M. (2008). Quantifying above-cloud aerosol using spaceborne lidar for improved understanding of cloudy-sky direct climate forcing. *J. Geophys. Res.* 113: D13206.
- Dey, S., Girolamo, L.D., van Donkelaar, A., Tripathi, S. N., Gupta, T. and Mohan, M. (2012). Variability of outdoor fine particulate ($PM_{2.5}$) concentration in the Indian Subcontinent: A remote sensing approach. *Remote Sens. Environ.* 127: 153–161.
- Forouzanfar, M.H., Alexander, L., Anderson, H.R., Bachman, V.F., Biryukov, S., et al. (2015). Global, regional, and national comparative risk assessment of 79 behavioral, environmental and occupational, and metabolic risks or clusters of risks in 188 countries, 1990–2013: A systematic analysis for the Global Burden of Disease Study 2013. *Lancet* 386: 2287–2323.
- Giglio, L., Descloitres, J., Justice, C.O. and Kaufman, Y. (2003). An enhanced contextual fire detection algorithm for MODIS. *Remote Sens. Environ.* 87: 273–282.
- Giglio, L., Schroeder, W. and Justice, C. O. (2016). The collection 6 MODIS active fire detection algorithm and fire products. *Remote Sens. Environ.* 78: 31–41.
- Girolamo, L., Bond, T.C., Bramer, D., Diner, D.J., Fettinger, F., Kahn, R.A., Martonchik, J.V., Ramana, M.V., Ramanathan, V. and Rasch, P.J. (2004). Analysis of multiangle imaging spectro-radiometer (MISR) aerosol optical depths over greater India during winter 2001–2004. *Geophys. Res. Lett.* 31: L23115.
- HEI (Health Effects Institute) (2004). Health effects of outdoor air pollution in developing countries of Asia: A literature review. Special Report 15. Health Effects Institute, Boston, <https://www.healtheffects.org/publications>.
- HEI (Health Effects Institute) (2008). Public health and air pollution in Asia: Science access on the net (PAPA-SAN). <https://www.healtheffects.org/publications>.
- Hsu, N.C., Jeong, M.J., Bettenhausen, C., Sayer, A.M., Hansell, R., Seftor, C.S., Huang, J. and Tsay, S.C. (2013). Enhanced Deep Blue aerosol retrieval algorithm: The second generation. *J. Geophys. Res. Atmos.* 118: 9296–9315.
- Jain, N., Bhatia, A. and Pathak, H. (2014). Emission of Air Pollutants from Crop Residue Burning in India. *Aerosol Air Qual. Res.* 14: 422–430.
- Jethva, H., Torres, O. and Ahn, C. (2014a). Global assessment of OMI aerosol single-scattering albedo using ground-based AERONET inversion. *J. Geophys. Res. Atmos.* 119: 9020–9040.
- Jethva, H., Torres, O., Waquet, F., Chand, D. and Hu, Y. (2014b). How do A-train sensors intercompare in the retrieval of above-cloud aerosol optical depth? A case study-based assessment. *Geophys. Res. Lett.* 41: 186–192.
- Kanamitsu, M. (1989). Description of the NMC global data assimilation and forecast system. *Weather Forecasting* 4: 335–342.
- Kaskaoutis, D.G., Kumar, S., Sharma, D., Singh, R.P., Kharol, S.K., Sharma, M., Singh, A.K., Singh, S., Singh, A. and Singh, D. (2014). Effects of crop residue burning on aerosol properties, plume characteristics, and long-range transport over northern India. *J. Geophys. Res. Atmos.* 119: 5424–5444.
- Leeuwen, F.X. and Rolaf, V. (2002). A European perspective on hazardous air pollutants. *Toxicology* 181–182: 355–359.
- Levy, R.C., Remer, L.A. and Dubovik, O. (2007). Global aerosol optical properties and application to Moderate Resolution Imaging Spectroradiometer aerosol retrieval over land. *J. Geophys. Res.* 112: D13210.
- Lyapustin, A., Wang, Y., Laszlo, I., Kahn, R., Korkin, S., Remer, L., Levy, R. and Reid, J.S. (2011). Multiangle implementation of atmospheric correction (MAIAC): 2. Aerosol algorithm, *J. Geophys. Res.* 116: D03211.
- Lyapustin, A., Korkin, S., Wang, Y., Quayle, B. and Laszlo, I. (2012). Discrimination of biomass burning smoke and clouds in MAIAC algorithm. *Atmos. Chem. Phys.* 12: 9679–9686.
- Mhawish, A., Sorek-Hamer, M., Banerjee, T., Lyapustin, A., Broday, D.M. and Chatfield, R. (2018). Inter-comparison and evaluation of MODIS C6 MAIAC, DB and DT AOD over South Asia. *Remote Sens. Environ.*, Submitted.
- Mishra, A.K. and Shibata, T. (2012). Synergistic analyses of optical and microphysical properties of agricultural crop residue burning aerosols over the Indo-Gangetic Basin (IGB). *Atmos. Environ.* 57: 205–218.
- Mittal, S.K., Singh, N., Agarwal, R., Awasthi, A. and Gupta, P.K. (2009). Ambient air quality during wheat and rice crop stubble burning episodes in Patiala. *Atmos. Environ.* 43: 238–244.
- Pope, C.A. III, Ezzati, M. and Dockery, D.W. (2009). Fine-particulate air pollution and life expectancy in the United States. *N. Engl. J. Med.* 360: 376–386.
- Rajput, P., Sarin, M., Sharma, D. and Singh, D. (2014). Characteristics and emission budget of carbonaceous

- species from post-harvest agricultural-waste burning in source region of the Indo-Gangetic Plain. *Tellus B* 66: 1.
- Rolph, G.D. (2017). Real-time Environmental Applications and Display sYstem (READY) Website (<http://www.ready.noaa.gov>). NOAA Air Resources Laboratory, College Park, MD.
- Sayer, A.M., Munchak, L.A., Hsu, N.C., Levy, R.C., Bettenhausen, C. and Jeong, M.J. (2014). MODIS Collection 6 aerosol products: Comparison between Aqua's e-Deep Blue, Dark Target, and "merged" data sets, and usage recommendations. *J. Geophys. Res. Atmos.* 119: 13965–13989.
- Simpson, R., Denison, L., Petroeshevsky, A., Thalib, L. and Williams, G. (2000). Effects of ambient particle pollution on daily mortality in Melbourne, 1991–1996. *J. Exposure Anal. Environ. Epidemiol.* 10: 488–496.
- Singh, R.P. and Kaskaoutis, D.G. (2014). Crop residue burning: A threat to south Asian air quality. *Eos Trans. AGU* 95: 333.
- Stein, A.F., Draxler, R.R., Rolph, G.D., Stunder, B.J.B., Cohen, M.D. and Ngan, F. (2015). NOAA's HYSPLIT atmospheric transport and dispersion modeling system. *Bull. Amer. Meteor. Soc.* 96: 2059–2077.
- Stocker, T., Qin, D., Plattner, G.K., Tignor, M., Allen, S., Boschung, J., Nauels, A., Xia, Y., Bex, V. and Midgley, P. (2013). *IPCC, 2013: Climate Change 2013: The physical science basis*. Contribution of Working Group I to the Fifth Assessment Report of the Intergovernmental Panel on Climate Change, Cambridge University Press, Cambridge, United Kingdom and New York, NY, USA.
- TERI (2001). Review of past and on-going work on urban air quality in India. Report submitted to the World Bank, December, Tata Energy Research Institute, 2001EE41.
- Torres, O., Tanskanen, A., Veihelmann, B., Ahn, C., Braak, R., Bhartia, P.K., Veefkind, P. and Levelt, P. (2007). Aerosols and surface UV products from Ozone Monitoring Instrument observations: An overview. *J. Geophys. Res.* 112: D24S47.
- Torres, O., Ahn, C. and Chen, Z. (2013). Improvements to the OMI near-UV aerosol algorithm using A-train CALIOP and AIRS observations. *Atmos. Meas. Tech.* 6: 3257–3270.
- Torres, O., Bhartia, P.K., Herman, J.R., Ahmad, Z. and Gleason, J. (1998). Derivation of aerosol properties from satellite measurements of backscattered ultraviolet radiation: Theoretical basis. *J. Geophys. Res.* 103: 17099–17110.
- van Donkelaar, A., Martin, R.V., Brauer, M. and Boys, B.L. (2015). Use of satellite observations for long-term exposure assessment of global concentrations of fine particulate matter. *Environ. Health Perspect.* 123: 135–143.
- Venkataraman, C., Habib, G., Kadamba, D., Shrivastava, M., Leon, J.F., Crouzille, B., Boucher, O. and Streets, D.G. (2006). Emissions from open biomass burning in India: Integrating the inventory approach with high-resolution Moderate Resolution Imaging Spectroradiometer (MODIS) active-fire and land cover data. *Global Biogeochem. Cycles* 20: GB2013.
- WHO (2000). Guidelines for air quality, World Health Organization, Geneva (2000) World Health Statistics 2014. World Health Organization. http://www.who.int/gho/publications/world_health_statistics/2014/en/
- WHO (2014). Ambient (outdoor) air pollution in cities database 2014, http://www.who.int/phe/health_topics/outdoorair/databases/cities-2014/en/.
- WHO (2016). WHO global urban ambient air pollution database (update 2016), http://www.who.int/phe/health_topics/outdoorair/databases/cities/en/.
- Winker, D.M., Hunt, W.H. and McGill, M.J. (2007). Initial performance assessment of CALIOP. *Geophys. Res. Lett.* 34: L19803.
- Winker, D.M., Vaughan, M.A., Omar, A., Hu, Y., Powell, K.A., Liu, Z., Hunt, W.H. and Young, S.A. (2009). Overview of the CALIPSO mission and CALIOP data processing algorithms. *J. Atmos. Oceanic Technol.* 26: 2310–2323.
- Young, S.A. and Vaughan, M.A. (2009). The retrieval of profiles of particulate extinction from Cloud Aerosol Lidar Infrared Pathfinder Satellite Observations (CALIPSO) data: Algorithm description. *J. Atmos. Oceanic Technol.* 26: 1105–1119.

Received for review, December 19, 2017

Revised, March 29, 2018

Accepted, April 28, 2018